Eur. J. Mineral., 38, 217–229, 2026
https://doi.org/10.5194/ejm-38-217-2026

European Journal of Mineralogy
Open Access

Lopatkaite, a new mineral from Taylor Pit, Madoc, Ontario, Canada

Dan Topa[1], **Emil Makovicky**[2], **Hubert Putz**[3], **and Georg Zagler**[4]

[1]Mineralogisch-Petrographische Abteilung, Naturhistorisches Museum, Burgring 7, 1010 Wien, Austria
[2]Department of Geoscience and Resource Management, University of Copenhagen, Østervoldgade 10, 1350, Copenhagen K, Denmark
[3]Salletmayr & Friedl Ziviltechniker GmbH, Karl-Lötsch-Straße 10, 4840 Vöcklabruck, Austria
[4]Brandirn 21, 5222 Munderfing, Austria

Correspondence: Dan Topa (dan.topa@nhm.at)

Received: 18 December 2025 – Revised: 7 April 2026 – Accepted: 8 April 2026 – Published: 23 April 2026

Abstract. Lopatkaite, ideally $Pb_{10}As_2Sb_6S_{22}$ ($Z = 4$), is a new arsenic-bearing sulfosalt found in the Madoc deposit, Taylor Pit, Ontario, Canada. Associated minerals in the holotype specimen are boulangerite, veenite, and sterryite, all embedded in a calcite matrix. Lopatkaite is greyish black and opaque, with metallic lustre and dark-grey streak. It is brittle without any discernible cleavage and parting and has a Mohs hardness of 3–3.5. In reflected light lopatkaite is greyish white, with distinct bireflectance and pleochroism from white to grey, especially in oil. Under crossed polarisers, anisotropism is distinct, with rotation tints in shades of grey. Reflectance measurements in air yield the following R_{min}/R_{max} values based on the standard wavelengths (Commission on Ore Mineralogy, COM): 37.0 % / 39.3 % (470 nm), 34.1 % / 36.9 % (546 nm), 33.1 % / 36.2 % (589 nm), and 31.3 % / 34.1 % at (650 nm). The average result of four electron probe microanalyses for the structurally investigated grain is as follows (in wt %): Pb 57.81(4), As 3.53(8), Sb 20.03(6), S 19.08(6), and total 100.46(22), corresponding to $Pb_{10.28(3)}As_{1.74(4)}Sb_{6.06(3)}S_{21.92(3)}$ (based on $18Me + 22S = 40$ atoms per asymmetric unit). The density calculated using the empirical formula is 6.168 Mg m^{-3}. Single-crystal X-ray diffraction data show lopatkaite to be monoclinic, space group $P2_1/c$ (no. 14), with $a = 8.0806(6)$, $b = 23.3597(18)$, $c = 21.4880(16)$ Å, $\beta = 100.7090(10)°$, $V = 3985.4(5)$ Å^3, and $Z = 4$. The seven strongest lines in the (calculated) powder diffraction pattern are as follows (d in Å (intensity) (hkl)): 3.728(39) 211, 3.712(100) 035, 3.653(35) 062, 2.804(41) −261, 2.780(43) 260, 2.779(38) −262, and 2.020(47) −402. The ideal formula is in accordance with the results of the crystal structure analysis, $Pb_{10.336}As_{1.567}Sb_{6.088}S_{22}$, and may be derived from the ideal boulangerite formula, $Pb_{10}Sb_8S_{22}$ ($Z = 4$), by means of substitution of two Sb atoms with two As atoms. Lopatkaite is an isotype of boulangerite, differing by dominant As occupancy at two crystallographically independent mixed (Sb, As) sites. This dominant-site substitution defines lopatkaite as the arsenic-dominant isotype of boulangerite and justifies its recognition as a distinct mineral species. Lopatkaite is also a new member of the rod-based family of sulfosalts.

1 Introduction

Boulangerite is a common mineral and a prominent member of the family of rod-based structures (Makovicky, 1993), present in many hydrothermal lead mineralisations. The single-crystal X-ray diffraction studies on natural ordered boulangerite of Mumme (1989) and Ventruti et al. (2012) show a monoclinic system; space group $P2_1/a$; and unit-cell parameters $a = 21.61$, $b = 23.54$, $c = 8.08$ Å, $\beta = 100.71°$ and $a = 21.554(4)$, $b = 23.454(4)$, $c = 8.079$ Å, and $\beta = 100.76(1)°$. The ideal formula is $Pb_{10}Sb_8S_{22}$ ($Z = 4$), reflecting the presence of 18 cation and 22 anion independent sites in the structure.

In contrast, the single-crystal X-ray diffraction studies on a synthetic phase with similar chemistry to boulangerite, de-

scribed by Petrova et al. (1978) and Skowron and Brown (1990), yielded space group *Pbnm* and unit-cell parameters $a = 21.40(1)$, $b = 23.51(1)$, and $c = 4.036(1)$ Å and space group *Pnam* and unit-cell parameters $a = 23.490(5)$, $b = 21.245(1)$, and $c = 4.020(1)$ Å, respectively. The ideal formula is $Pb_5Sb_4S_{11}$ ($Z = 4$), reflecting the presence of 9 cation and 11 anion independent sites in the structure. The synthetic phase is a disordered orthorhombic phase with $c \sim 4.02$ Å (i.e. half of c of natural boulangerite) and should not be named boulangerite but rather a "boulangerite-like" phase.

Arsenic is a known minor component in boulangerite, but most published analyses show limited substitution of Sb with As, with atomic As / (As + Sb) ratios that are typically below 0.125. For example, Jambor et al. (1982) quote a ratio of 0.125 (i.e. 2.02 As wt %) for As-bearing boulangerite from Madoc, Orlandi et al. (2008) describe boulangerite from Bottino with As / (As + Sb) equal to 0.106 (i.e. 1.7 As wt %), Ventruti et al. (2012) found boulangerite to have the highest As / (As + Sb) atomic ratio of only 0.0144 at this locality (i.e. 0.24 As wt %), while Birnie and Petersen (1977) describe ratios of As / (As + Sb) (in apfu) as high as 0.36 (i.e. 5.97 As wt %) in samples from the Lichito I vein of Huachocolpa, Peru.

Substantial arsenic concentrations in other sulfosalts have been observed in zinkenite (4.4 As wt % in Jas Roux, Johan and Mantienne (2000); from 0.0 wt % to 11.5 wt % in the Hemlo gold deposit, Harris (1989); and up to 7.6 wt % in the Vorontsovskoe gold deposit, Kasatkin et al., 2022), tsugaruite (∼ 12.5 As wt %, Shimizu et al., 1998, and Biagioni et al., 2021), vurroite (∼ 8.4 As wt %, Garavelli et al., 2005), tazieffite (∼ 9.7 As wt %, Zelenski et al., 2009), the sterryite group (from 2.8 As wt % to 8.3 As wt %, Moëlo et al., 2011; Bindi et al., 2016, and Biagioni et al., 2016), chovanite (3.37 wt %, Biagioni and Moëlo, 2017), and ginelfite (6.2 wt %, Biagioni et al., 2025). The single-crystal studies show that arsenic plays an important role in the crystal structure and the crystal chemistry (due to the As-dominant site or sites) of the aforementioned minerals, except for zinkenite. Low contents of As, as in andreadiniite (1.57 wt %) in the study of Biagioni et al. (2018) and launayite (2.7 wt %) in the study of Topa et al. (2025), were shown to play no structural role. The structural role of As in sorbyite (up to 6.2 wt %), playfairite (up to 3.3 wt %), and madocite (up to 3.1 wt %) as described by Jambor et al. (1982) remains unknown.

Here we describe in detail the new mineral lopatkaite, a high-arsenic-bearing analogue of boulangerite, from Madoc, Ontario, Canada. The new mineral is named after Eduard Lopatka (born 1961), who provided to us his sample collection of Madoc material, in which we found the new mineral.

The new mineral species and name were approved by the Commission on New Minerals Nomenclature and Classification of the International Mineralogical Association (IMA 2012-83; Topa et al., 2013). The holotype, consisting of a polished sample, was deposited in the mineralogical collection of the Natural History Museum, Vienna, Austria, under catalogue number O 3954 (note: the holotype was originally deposited in the collection of the Department of Materials Engineering and Physics, University of Salzburg, Salzburg, Austria, under catalogue number 15008 but was later transferred to Vienna).

2 Occurrence, appearance, and physical properties

The type locality of lopatkaite is the classical sulfosalt occurrence at the Taylor Pit in Madoc, Ontario, which was described previously by Jambor (1967a, b) and Jambor et al. (1982). Sulfosalts occur there in steeply dipping *cipollino* calcite–dolomite marbles near their contact with Precambrian granite. The bulk of sulfides is composed of dark-brown sphalerite, boulangerite, jamesonite, and fine-grained arsenopyrite and pyrite. A variety of rare sulfosalts (Jambor, 1967a, b) occur sparingly, intergrown with the just mentioned ones, and they are difficult to identify. They comprise semseyite, bournonite, playfairite, launayite, madocite, twinnite, veenite, guettardite, Sb-bearing baumhauerite, and tetrahedrite. They were identified in and described for this locality in the quoted publications.

Jambor et al. (1982) suggest that As-rich mineralisation came first at Madoc, followed by an Sb-rich one. The association galena–pyrite–sphalerite might be of synsedimentary origin, whereas hydrothermal activity connected with the intrusion of nearby granite plutons into the metamorphosed limestone triggered the formation of sulfosalts.

In the investigated samples, lopatkaite forms grains which attain a size of up to 300 µm and grain aggregates reaching up to more than 500 µm across. Grains of lopatkaite are embedded in calcite and are subhedral to anhedral. Neither distinct crystal forms nor twinning were observed. Enveloping by later boulangerite partly leaves traces of original crystal shape and partly leads to heavily corroded grains enclosed in boulangerite (Fig. 1). The colour is greyish black, with metallic lustre and dark-grey streak. Lopatkaite is opaque with a Mohs hardness (derived from the indentation measurements) of 3–3.5; VHN_{50} data are as follows: a range of 189–208 and a mean of 200 kg mm^{-2}. Lopatkaite is brittle, without observed cleavage and parting. The density could not be measured because of the paucity of available pure material; the density (calc.) is equal to 6.168 Mg m^{-3} using the empirical formula and 6.096 Mg m^{-3} using the ideal formula. The $a : b : c$ ratio calculated from the unit-cell parameters is 0.683 : 1 : 0.429.

In reflected light under one polariser, the colour is greyish white. No internal reflections were observed, and pleochroism or bireflectance is distinct and white to dark grey, especially in oil. Anisotropy is distinct, with rotation tints in shades of grey. Quantitative data on reflectance were obtained by means of a WTiC standard and Leitz MPV-SP microscope photometer and are given in Table 1.

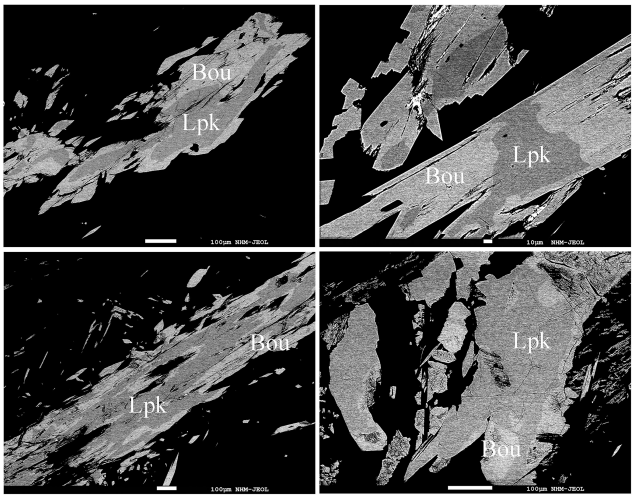

Figure 1. Backscattered electron images of skeletal crystals and grains of lopatkaite (Lpk) enclosed in, and partly replaced by, boulangerite (Bou).

Table 1. Reflectance values (WTiC standard in air) for lopatkaite from Madoc. The values corresponding to wavelengths, recommended by the Commission of Ore Mineralogy of IMA, are marked in bold.

λ (nm)	R_{min}	R_{max}	λ (nm)	R_{min}	R_{max}
400	34.5	35.1	560	34.0	36.6
420	37.1	39.6	580	33.3	36.4
440	37.7	39.8	**589**	**33.1**	**36.2**
460	37.4	39.8	600	32.8	35.9
470	**37.0**	**39.3**	620	32.0	35.2
480	36.7	39.2	640	31.5	34.4
500	35.7	38.2	**650**	**31.3**	**34.1**
520	34.9	37.3	660	31.3	34.0
540	34.2	37.0	680	30.7	33.8
546	**34.1**	**36.9**	700	30.3	33.3

3 Chemical composition

Chemical analyses of lopatkaite were carried out at the Central Research Laboratories of the Natural History Museum, Vienna, using a JEOL "Hyperprobe" JXA 8530F field emission gun electron probe microanalyser (FE-EPMA). The analytical conditions were as follows: WDS measuring mode, accelerating voltage of 25 kV, beam current of 20 nA, beam diameter of 1.5 µm, and count times of 10 s in peak position and 5 s in background positions. JEOL software was used for the acquisition and processing of data. The following emission lines and standards were used: As$L\alpha$ and Tl$L\alpha$ (lorándite, $TlAsS_2$), Pb$M\alpha$ (galena), Ag$L\alpha$ (Ag metal), Sb$L\alpha$ and S$K\alpha$ (stibnite), Hg$L\alpha$ (cinnabar), and Cu$K\alpha$ (chalcopyrite). Other elements such as Bi, Fe, and Hg were sought but not detected. Proper empirical correction was made for the interference of the third order of the Sb$L\alpha$ line with the analytical As$L\alpha$ line. Under the analytical conditions described, the detection limits for the measured elements in the lopatkaite matrix were as follows (expressed in wt %): S, Cu, and Fe ∼ 0.03; As, Ag, and Sb ∼ 0.06; and Hg, Tl, Pb, and Bi ∼ 0.09. Analytical data are given in Table 2.

The empirical formula (based on 40 apfu) is $Pb_{10.28}Sb_{6.06}As_{1.74}S_{21.92}$, leading to a simplified formula of $Pb_{10}Sb_6As_2S_{22}$, which requires the following (in wt %): 56.64 Pb, 19.97 Sb, 4.10 As, and 19.29 S, for a total 100.00. There are well-documented difficulties in obtaining the theoretical Pb / (Sb + As) ratio of 1.25 for a boulangerite-type structure, described in detail by Ventruti et al. (2012); explanations given for these problems vary between the correction problems of electron microanalyser programmes and the presence of structural defects in the rod-based sulfosalt structure, both without a valid and/or unambiguous proof.

4 X-ray crystallography

Powder X-ray diffraction data could not be collected due to a lack of suitable pure material and were instead calculated based on single-crystal structure determination results. The seven strongest lines are shown in Table 3.

4.1 X-ray single-crystal study

A fragment with irregular shape and 0.05 × 0.08 × 0.12 mm in size was mounted on a Bruker AXS three-circle diffractometer equipped with a charge coupled device (CCD) area detector. The SMART (Bruker AXS, 1998a) system of programmes was used for unit-cell determination and data collection, SAINT+ (Bruker AXS, 1998b) was used for the reduction in the intensity data, and XPREP (Bruker AXS, 1997) was used for space group determination and empirical absorption correction based on pseudo ψ scans. The centrosymmetric space group $P2_1/c$, proposed by the XPREP programme, was chosen. It is consistent with the monoclinic symmetry of the lattice and intensity statistics (mean $|E \cdot E - 1| = 1.195$ (expected values: 0.968 for the centrosymmetric case and 0.736 for non-centrosymmetric case)). We started the refinement process (using SHEXL; Bruker AXS, 1997) by adopting the atom coordinates of the monoclinic structure model published by Mumme (1989), with modified site labels. The introduction of a twin model through the matrix [−1 0 0 | 0 −1 0 | 1 0 1] did not improve the R index, as shown by a batch scale factor (BASF) of 0.0047(6) (i.e. no twinning within error limits). As in the Mumme model, we initially treated all cations (10 Pb and 8 Sb) as pure Pb and Sb sites. The analysis of their coordination characteristics and scattering function values indicated the following: a mixed (Pb, Sb) occupancy for the Pb4 site, a mixed (As, Sb) occupancy for the Sb3 and Sb8 sites, mixed (Sb, As) occupancies for the Sb4 and Sb7 sites, and a mixed (Sb, Pb) oc-

Table 2. Average chemical composition data (in wt %) for boulangerite (group 1), As-bearing boulangerite (group 2 to 4), and lopatkaite (group 5 and 6) from Madoc. Group 5 represents the average chemistry of the grain used for crystal structure determination, and group 6 is for a high-As lopatkaite. Empirical formulae are calculated based on 40 atoms per formula unit, apfu ($Me_{18}S_{22}$). Values in italics represent standard deviations for the last decimal.

	Boulangerite				Lopatkaite		
	Group 1	Group 2	Group 3	Group 4	Group 5	Group 6	Ideal formula
NA[a]	3	3	3	3	4	5	–
Pb	56.71(9)	56.29(1)	56.63(8)	57.40(2)	57.81(4)	57.36(6)	56.64
As	0.00(0)	1.63(13)	1.93(6)	2.56(8)	3.53(8)	4.43(7)	4.10
Sb	24.46(2)	23.08(21)	22.42(1)	20.98(1)	20.03(9)	18.77(13)	19.97
S	18.54(1)	18.90(1)	18.92(4)	18.94(3)	19.08(6)	19.20(1)	19.29
Total	99.71(11)	99.91(6)	99.90(2)	99.89(8)	100.46(22)	99.77(2)	100
ch[b]	−0.62(12)	−0.16(7)	−0.32(6)	−0.71(10)	0.27(38)	−0.33(7)	0
Pb	10.40(1)	10.13(1)	10.19(3)	10.32(2)	10.28(3)	10.17(1)	10
As	0.00(0)	0.81(7)	0.96(3)	1.27(4)	1.74(4)	2.17(3)	2
Sb	7.63(1)	7.07(7)	6.86(1)	6.42(1)	6.06(3)	5.66(4)	6
S	21.97(1)	21.99(1)	21.99(1)	21.99(1)	21.92(3)	21.99(1)	22
As/Sb	0	0.115	0.140	0.199	0.287	0.383	0.333
Sb + As	7.63	7.88	7.83	7.69	7.82	7.83	8
ΣMe[c]	18.03	18.01	18.01	18.01	18.08	18.01	18
Pb / (Sb + As)	1.36	1.29	1.30	1.34	1.32	1.30	1.25
Sb / (Sb + As)	1.00	0.90	0.88	0.83	0.795	0.723	0.75

[a] Number of point analyses. [b] *ch* denotes charge-balance values calculated as ($\sum$*cation valence* − $\sum$*anion valence*) using atom per cent values. [c] Although ∑Me is almost equal to the theoretical value of 18, the ratio Pb / (Sb + As), ranging from 1.29 to 1.36, departs from the theoretical value of 1.25 (see the text for a discussion).

cupancy for the Sb5 and Sb6 sites of Mumme's model. The structure formula obtained is $Pb_{10.336}As_{1.567}Sb_{6.088}S_{22}$.

The final stage of refinement with anisotropic displacement parameters for all cation and anion sites converged to $R_1 = 0.0412$ [3569 reflections with $F_o > 4\sigma(F_o)$] and showed no evidence of disorder comparable to that reported for the orthorhombic synthetic "boulangerite-like" phase. Details about crystal data, as well as data collection and refinement, are given in Table 4. The relatively low resolution of the dataset ($2\theta_{max} = 41.62°$) reflects the improper conditions of data collection for the available crystal from Madoc. Despite this limitation, the refinement converged to a stable and chemically consistent structural model, supported by agreement with chemical data and bond-valence analysis. A separate study, currently in preparation, will address material from other localities, including datasets collected at a higher resolution ($2\theta_{max}$ up to ∼ 57°). Fractional coordinates, site occupancies, anisotropic displacement parameters, charge distribution, and bond-valence sum values are compiled in Table 5. Table 6 reports selected cation–anion bond distances. Full details are given in the lopatkaite.CIF and lopatkaite_checkCIF.pdf files, both deposited in the Supplement (S1 and S2).

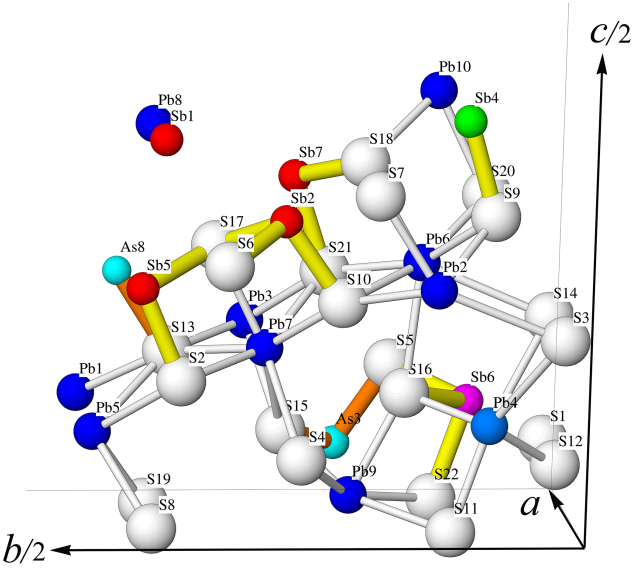

Figure 2. Atom labelling in the asymmetric unit of lopatkaite. White: S sites; dark blue: Pb sites; light blue: (Pb, Sb) site; turquoise: As-dominant sites; red: Sb sites (Sb7 included); purple (Sb, Pb) site; and green: (Sb, As) site.

Table 3. Calculated X-ray powder diffraction data (d in Å) for lopatkaite from Madoc*.

I_{rel}	d_{calc}/Å	h	k	l	I_{rel}	d_{calc}/Å	h	k	l	I_{rel}	d_{calc}/Å	h	k	l
5	15.66	0	1	1	15	2.969	2	3	3	5	2.031	2	0	8
4	7.83	0	2	2	15	2.964	−2	3	5	5	2.027	−2	0	10
10	6.74	0	1	3	7	2.937	2	5	1	**47**	**2.020**	**−4**	**0**	**2**
6	6.03	0	2	3	7	2.934	−2	5	3	3	1.9991	2	5	7
4	5.56	−1	3	1	9	2.835	2	2	4	4	1.9958	−2	5	9
4	4.81	0	2	4	7	2.829	−2	2	6	5	1.9580	0	8	8
5	4.56	0	5	1	7	2.814	0	8	2	8	1.9181	2	4	8
7	4.37	0	3	4	21	2.814	2	4	3	7	1.9148	−2	4	10
4	4.13	1	4	2	30	2.813	0	3	7	4	1.9130	0	1	11
3	4.06	1	0	4	25	2.810	−2	4	5	3	1.8636	−2	1	11
6	3.971	0	2	5	**41**	**2.804**	**−2**	**6**	**1**	22	1.8565	2	9	5
4	3.970	2	0	0	**43**	**2.780**	**2**	**6**	**0**	8	1.8560	0	6	10
7	3.967	−2	0	2	**38**	**2.779**	**−2**	**6**	**2**	21	1.8545	−2	9	7
8	3.916	0	4	4	10	2.711	2	6	1	3	1.8510	2	11	1
16	3.914	2	1	0	10	2.709	−2	6	3	3	1.8503	−2	11	3
16	3.911	−2	1	2	19	2.680	0	4	7	11	1.7759	4	3	3
7	3.893	0	6	0	9	2.647	2	5	3	12	1.7729	−4	3	7
22	3.892	0	5	3	7	2.643	−2	5	5	4	1.7684	4	6	0
19	3.829	0	6	1	6	2.574	0	2	8	3	1.7672	−4	6	4
5	3.759	2	2	0	5	2.514	2	3	5	5	1.7595	0	0	12
4	3.756	−2	2	2	5	2.509	−2	3	7	5	1.7537	−2	12	1
39	**3.728**	**2**	**1**	**1**	3	2.435	0	9	3	4	1.7525	−2	10	7
34	3.722	−2	1	3	9	2.418	2	7	2	5	1.7492	0	10	8
100	**3.712**	**0**	**3**	**5**	8	2.415	−2	7	4	4	1.7478	2	12	0
35	**3.653**	**0**	**6**	**2**	21	2.369	2	2	6	4	1.7476	−2	12	2
4	3.507	2	0	2	21	2.364	−2	2	8	7	1.7411	0	13	3
5	3.468	2	1	2	6	2.334	0	1	9	3	1.7364	0	11	7
6	3.462	−2	1	4	11	2.329	0	9	4	4	1.7227	−4	7	1
11	3.422	0	4	5	3	2.314	2	7	3	5	1.7221	−4	7	3
4	3.359	2	2	2	7	2.310	2	8	1	6	1.7216	0	6	11
4	3.358	−1	5	4	7	2.309	−2	8	3	5	1.7108	4	3	4
6	3.353	−2	2	4	11	2.244	2	8	2	4	1.7077	−4	3	8
34	3.296	0	7	1	11	2.242	−2	8	4	3	1.6796	4	4	4
33	3.207	0	3	6	6	2.211	0	9	5	5	1.6766	−4	4	8
7	3.198	2	3	2	7	2.173	2	2	7	5	1.6481	0	14	2
9	3.193	−2	3	4	6	2.169	−2	2	9	5	1.6424	4	3	5
4	3.025	2	5	0	4	2.149	2	5	6	4	1.6392	−4	3	9
4	3.024	−2	5	2	3	2.145	−2	5	8	3	1.6147	4	4	5
30	3.014	0	4	6	18	2.136	0	10	4	3	1.5849	2	6	10
32	3.007	2	4	2	3	2.111	0	0	10	3	1.5826	−2	6	12
31	3.002	−2	4	4	8	2.044	0	10	5	4	1.4684	4	10	2

* The theoretical pattern was calculated using PowderCell 2.3 (Kraus and Nolze, 1996) in Debye–Scherrer configuration employing Cu$K\alpha$ radiation ($\lambda = 1.540598$ Å), a fixed slit, and no anomalous dispersion. Unit-cell parameters, space group, atom positions, site occupancy factors, and equivalent displacement factors from the crystal-structure determination were used. The seven strongest lines are indicated in bold.

5 Description of the structure

The structure of lopatkaite contains 18 distinct coordination polyhedra of cations and 22 anions (Table 5, Fig. 3). The asymmetric unit contains nine Pb sites, one mixed (Pb, Sb) site, two Sb sites, two mixed (As, Sb) sites with occupancy values of 0.67–0.58 As and 0.33–0.42 Sb, two mixed (Sb, As) sites, and two mixed (Sb, Pb) sites. Similarly to the closely related boulangerite, the lopatkaite structure (Fig. 4) is isotypic with the MDO1 polytype described by Ventruti et al. (2012) and contains large rod-like modules based on an SnS archetype described by Makovicky (1993) and Ferraris et al. (2008) and Moëlo et al. (2008).

The asymmetric unit content is presented in Fig. 2, and the crystal structure is shown in Fig. 3, in which the rods are outlined by shading in green. Figure 3 shows that the struc-

Table 4. Crystal data, data collection information, and refinement details for lopatkaite from Madoc.

Crystal data	
Crystal size (mm)	$0.05 \times 0.08 \times 0.12$
Space group	$P2_1/c$
a (Å)	8.0806(6)
b (Å)	23.3597(18)
c (Å)	21.4880(16)
β (°)	100.7090(10)
V (Å^3)	3985.4(5)
Data collection and refinement	
Radiation, wavelength (Å)	Mo$K\alpha$, $\lambda = 0.71073$
Temperature (K)	300(2)
$2\theta_{max}$ (°)	41.62
Measured reflections	25 691
Unique reflections	4241
Reflections with $F_o > 4\sigma(F_o)$	3569
R_{int}	0.1295
R_σ	0.0632
Range of h, k, l	$-8 \le h \le 8$ $-23 \le k \le 23$ $-21 \le l \le 21$
R_1 [$F_o > 4\sigma(F_o)$]	0.0412
R (all data)	0.0498
wR (on F_o^2)	0.0842
Goof	1.032
Number of refined parameters	369
Restraints	0
Maximum and minimum residual peak (e Å^{-3})	2.68 (at 1.76 Å from S1) −2.96 (at 0.25 Å from Sb1)

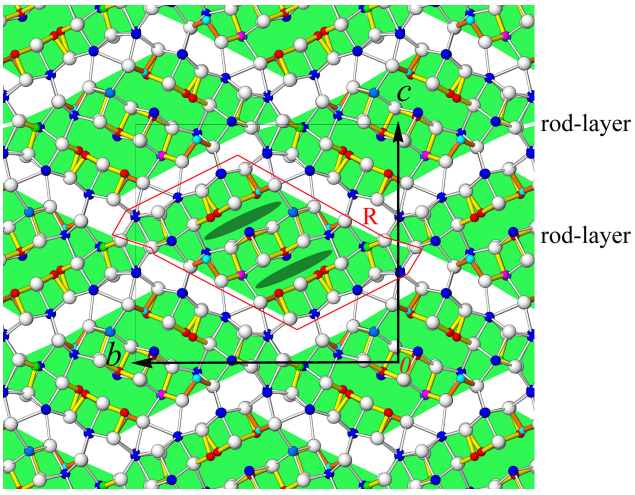

Figure 3. The crystal structure of lopatkaite viewed along [100]. Atom colouring is as in Fig. 2. Infinite lozenge-shaped rod layers along [100] and [010] of the SnS-like archetype, alternating along [001] with non-commensurate interspaces (uncoloured). The rod layer can be viewed as a repetition of a basic rod R (see Fig. 4) along the b axis. The lone electron pair (LEP) is indicated in dark-green colour.

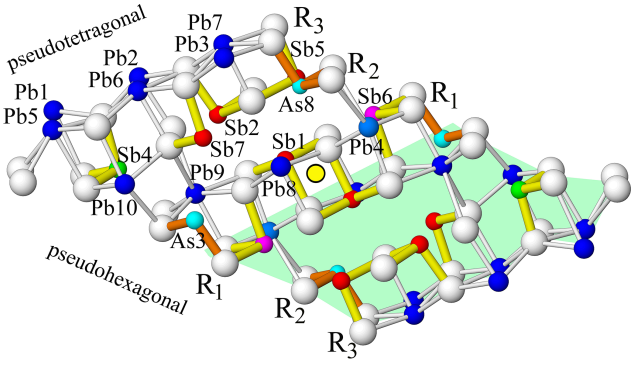

Figure 4. The independent sites of the rod R in the crystal structure of lopatkaite viewed along slightly inclined [100] and arranged in three double ribbons (R_1, R_2, R_3), each of them three polyhedra long. The symmetry centre which builds the whole rod is indicated. The mixed sites $(Sb_{0.723}As_{0.277})4$, $(Sb_{0.892}Pb_{0.108})5$, $(As_{0.581}Sb_{0.419})8$ in ribbon R_2 and $(As_{0.673}Sb_{0.327})3$, $(Pb_{0.922}Sb_{0.078})4$, and $(Sb_{0.694}Pb_{0.306})6$ in ribbon R_3 lie on the pseudohexagonal faces defined by S atoms. Atom colouring is as in Fig. 2.

ture consists of (001) ribbons composed of [100] rods with a lozenge-like cross-section. Each rod consists of three broad double ribbons separated by interspaces which accommodate lone electron pairs of Sb^{3+} and As^{3+} cations.

The independent sites of the asymmetric unit (Fig. 4) build three ribbons, R_1, R_2, and R_3, each being three polyhedra long. The ribbons R_1 and R_2 are equivalent to the "ribbon C" and "ribbon M", respectively, described by Ventruti et al. (2012).

Pure Pb sites (Pb1, 2, 3, 5, 6, 7) lie on ribbon R_3, which has a $(100)_{PbS}$ configuration. The Pb atoms and the S atoms form a pseudotetragonal surface (Fig. 5). Polyhedra centred by Pb1, Pb5, Pb3, and Pb7 are bicapped trigonal prisms (CN = 8), while polyhedra centred by Pb2 and Pb6 are monocapped trigonal prisms (CN = 7). The ribbon R_2 hosts a central Sb2–(Sb,Pb)7 column of coordination polyhedra and two marginal, mixed Sb5–(As,Sb)8 and (Sb,As)4–Pb10 columns of polyhedra. The central ribbon R_1 of the rod hosts a central Sb1-Pb8 column of coordination polyhedra, and two marginal, mixed (As,Sb)3–Pb9 and (Sb,As)4–(Pb,Sb)4 columns of polyhedra.

The other two surfaces of the rod are composed of S atoms in a periodically sheared pseudohexagonal arrangement (Fig. 4). These surfaces face the pseudotetragonal surfaces of the adjacent rods, which are occupied by Pb atoms (as mentioned above), and the inter-rod space (left blank in Fig. 3) accommodates a complicated pattern of long Pb–S distances and weak lone-electron-pair stereoactivity of Pb.

Table 5. Sites, site occupancy (s.o.), fractional atom coordinates, equivalent isotropic displacement parameters (in Å^2), charge distribution, bond-valence sum values, and coordination numbers for lopatkaite from Madoc.

Site	S.o.	x/a	y/b	z/c	U_{eq}	REF	CD	BVS	CN
Pb1	$Pb_{1.00}$	0.94534(9)	0.49856(3)	0.12152(4)	0.0205(2)	2	2.011	1.955	8
Pb2	$Pb_{1.00}$	0.02502(9)	0.15963(3)	0.30820(4)	0.0167(2)	2	1.959	2.114	7
Pb3	$Pb_{1.00}$	0.97783(9)	0.32475(3)	0.20541(4)	0.0181(2)	2	1.981	2.035	8
(Pb,Sb)4	$Pb_{0.922(8)}Sb_{0.078(8)}$	0.20151(10)	0.09607(3)	0.13299(4)	0.0228(4)	2.078	2.030	2128	7
Pb5	$Pb_{1.00}$	0.42863(9)	0.49900(3)	0.11197(4)	0.0214(2)	2	1.997	1.929	7
Pb6	$Pb_{1.00}$	0.52901(9)	0.15991(3)	0.30553(4)	0.0177(2)	2	1.976	1.994	8
Pb7	$Pb_{1.00}$	0.47928(10)	0.32148(3)	0.20766(4)	0.0215(2)	2	1.952	1.914	7
Pb8	$Pb_{1.00}$	0.84966(10)	0.43036(3)	0.44980(4)	0.0260(3)	2	2.062	2.037	7
Pb9	$Pb_{1.00}$	0.39628(10)	0.23276(3)	0.03721(4)	0.0240(2)	2	2.110	1.873	7
Pb10	$Pb_{1.00}$	0.86568(9)	0.13612(3)	0.48741(4)	0.0178(2)	2	2.096	1.937	7
Sb1	$Sb_{1.00}$	0.33089(16)	0.43632(6)	0.46807(6)	0.0189(4)	3	2.969	3.178	7
Sb2	$Sb_{1.00}$	0.30848(16)	0.30967(5)	0.37081(6)	0.0168(3)	3	3.020	3.264	7
(As,Sb)3	$\mathbf{As_{0.673(16)}Sb_{0.327(16)}}$	0.9009(2)	0.23184(8)	0.06377(9)	0.0243(8)	3	2.990	3.263	7
(Sb,As)4	$Sb_{0.723(15)}As_{0.277(15)}$	0.36022(17)	0.12070(6)	0.48643(7)	0.0133(6)	3	2.925	3.342	7
(Sb,Pb)5	$Sb_{0.892(9)}Pb_{0.108(9)}$	0.27566(17)	0.45733(5)	0.29345(6)	0.0252(7)	2.892	2.997	2.730	7
(Sb,Pb)6	$Sb_{0.694(9)}Pb_{0.306(9)}$	0.68198(14)	0.10269(5)	0.12905(6)	0.0317(6)	2.694	2.725	2.772	7
(Sb,As)7	$Sb_{0.955(15)}As_{0.045(15)}$	0.81773(16)	0.28385(5)	0.38909(6)	0.0155(6)	3	3.100	3.307	7
(As,Sb)8	$\mathbf{As_{0.581(15)}Sb_{0.419(15)}}$	0.7658(2)	0.46696(7)	0.28013(8)	0.0184(7)	3	3.101	3.399	6
S1	$S_{1.00}$	0.8970(6)	0.0148(2)	0.0662(2)	0.0169(12)				
S2	$S_{1.00}$	0.2206(6)	0.4164(2)	0.1864(2)	0.0142(12)				
S3	$S_{1.00}$	0.0230(6)	0.0271(2)	0.2472(2)	0.0180(12)				
S4	$S_{1.00}$	0.1418(6)	0.2920(2)	0.0968(2)	0.0225(13)				
S5	$S_{1.00}$	0.9428(6)	0.1752(2)	0.1546(2)	0.0208(13)				
S6	$S_{1.00}$	0.0682(6)	0.3759(2)	0.3344(2)	0.0154(12)				
S7	$S_{1.00}$	0.0687(6)	0.2223(2)	0.4180(2)	0.0141(12)				
S8	$S_{1.00}$	0.1550(6)	0.4444(2)	0.0149(2)	0.0162(12)				
S9	$S_{1.00}$	0.3070(6)	0.0929(2)	0.3760(2)	0.0152(12)				
S10	$S_{1.00}$	0.2639(6)	0.2501(2)	0.2766(2)	0.0133(11)				
S11	$S_{1.00}$	0.1390(6)	0.1351(2)	0.0105(2)	0.0135(12)				
S12	$S_{1.00}$	0.4167(6)	0.0190(2)	0.0710(2)	0.0162(12)				
S13	$S_{1.00}$	0.7167(6)	0.4137(2)	0.1875(2)	0.0152(12)				
S14	$S_{1.00}$	0.4691(6)	0.0279(2)	0.2443(2)	0.0207(13)				
S15	$S_{1.00}$	0.7051(6)	0.2938(2)	0.0935(2)	0.0201(13)				
S16	$S_{1.00}$	0.4608(6)	0.1760(2)	0.1546(2)	0.0183(13)				
S17	$S_{1.00}$	0.5162(6)	0.3743(2)	0.3281(2)	0.0145(12)				
S18	$S_{1.00}$	0.6042(6)	0.2193(2)	0.4202(2)	0.0158(12)				
S19	$S_{1.00}$	0.6071(6)	0.4371(2)	0.0131(2)	0.0169(12)				
S20	$S_{1.00}$	0.8096(6)	0.0846(2)	0.3663(2)	0.0149(12)				
S21	$S_{1.00}$	0.7615(6)	0.2518(2)	0.2792(2)	0.0140(12)				
S22	$S_{1.00}$	0.6260(6)	0.1388(2)	0.0164(2)	0.0161(12)				

* REF is the charge of the site obtained from refinement, and CD and BVS represent charge distribution and bond-valence sum values, respectively, calculated for the cation sites with the programme ECoN21 (Ilinca, 2022). Bold lettering indicates As-dominant site labelling and occupancies.

Its character is very different from the regular lone-electron-pair spaces inside a rod layer (Fig. 3).

Along the 8 Å *a* direction (Fig. 5), the (As,Sb)3 sites alternate with Pb9 sites; the (Sb,As)4 sites alternate with Pb10 sites; and the third of the mixed sites, (As,Sb)8, alternates with the Sb5 site. The bonding pattern is that which is typical of Sb sulfosalts: no crankshaft chains are present (Fig. 5), but an Sb2–Sb5 pair connected via a short S–S edge and via shorter Sb–S distances is present, whereas Sb7 and (As,Sb)8 share a common long edge of their coordination polyhedra. Only Sb1 is top-bonded; the rest of Sb and As atoms are side-bonded, as can be seen from the short Sb–S distances in Fig. 4.

The atoms Sb7 and Sb8 have typical short Sb–S bond lengths (2.33–2.44 Å) in relation to the vertex of the coordination pyramid and 2.47 ± 0.01 Å at its base (Table 6), whereas those of Sb1 and Sb6 are longer than expected for the pyramidal base (2.55–2.61 and 2.61–2.66 Å, respec-

Table 6. Selected bond lengths (Å) for lopatkaite from Madoc.

Pb1-		Pb2-		Pb3-		(Pb,Sb)4-		Pb5-	
S20	2.800(5)	S7	2.742(5)	S13	2.935(5)	S11	2.742(5)	S20	2.874(5)
S3	2.863(5)	S20	2.910(5)	S6	2.982(5)	S16	2.780(5)	S8	3.025(5)
S9	3.010(5)	S9	2.917(5)	S2	2.982(5)	S5	2.893(5)	S9	3.040(5)
S2	3.070(4)	S21	3.011(5)	S4	2.990(5)	S12	2.984(5)	S19	3.041(5)
S8	3.185(5)	S10	3.023(5)	S15	3.032(5)	S1	3.226(5)	S14	3.119(5)
S13	3.214(5)	S5	3.263(5)	S10	3.067(5)	S14	3.318(5)	S19	3.134(5)
S8	3.340(5)	S3	3.360(5)	S21	3.084(5)	S3	3.467(5)	S2	3.179(5)
S19	3.548(5)			S5	3.654(5)			S13	3.259(5)
Pb6-		Pb7-		Pb8-		Pb9-		Pb10-	
S18	2.794(5)	S17	2.832(5)	S1	2.772(5)	S16	2.812(5)	S20	2.826(5)
S20	2.973(5)	S13	2.969(5)	S11	2.893(5)	S15	2.933(5)	S19	2.833(5)
S21	2.974(5)	S21	2.986(5)	S1	2.908(5)	S4	2.959(5)	S8	2.973(5)
S10	2.986(5)	S10	2.994(5)	S12	2.960(5)	S22	2.963(5)	S18	3.032(5)
S9	2.995(5)	S2	3.023(5)	S22	2.980(5)	S11	3.069(5)	S7	3.143(5)
S16	3.209(5)	S4	3.343(5)	S6	3.537(5)	S18	3.460(5)	S15	3.265(5)
S14	3.352(5)	S15	3.380(5)	S17	3.633(5)	S7	3.486(5)	S4	3.373(5)
		S16	3.580(5)						
Sb1-		Sb2-		(As,Sb)3-		(Sb,As)4-		(Sb,Pb)5-	
S12	2.427(5)	S10	2.429(5)	S15	2.320(5)	S19	2.389(5)	S2	2.456(5)
S11	2.558(5)	S6	2.492(5)	S5	2.330(5)	S8	2.412(5)	S17	2.748(5)
S1	2.606(5)	S17	2.553(5)	S4	2.399(5)	S9	2.419(5)	S6	2.785(5)
S22	2.987(5)	S7	3.111(5)	S22	3.140(5)	S7	3.472(5)	S14	2.873(5)
S12	3.038(5)	S18	3.217(5)	S11	3.307(5)	S18	3.502(5)	S3	2.909(5)
S6	3.533(5)	S11	3.752(5)	S18	3.718(5)	S4	3.802(6)	S12	3.748(5)
S17	3.881(5)	S22	3.852(5)	S7	3.793(5)	S15	3.830(5)	S1	3.796(5)
(Sb,Pb)6-		(Sb,As)7-		(As,Sb)8-					
S22	2.523(5)	S21	2.437(5)	S13	2.318(5)				
S16	2.606(5)	S7	2.470(5)	S14	2.353(5)				
S5	2.680(5)	S18	2.475(5)	S3	2.368(5)				
S12	2.997(5)	S17	3.307(5)	S17	3.253(5)				
S1	3.152(5)	S6	3.314(5)	S6	3.286(5)				
S14	3.704(5)	S11	3.823(5)	S12	3.955(5)				
S3	3.816(5)	S22	3.837(5)						

tively). The (Sb,Pb)5 and (Sb,Pb)6 sites have a bonding scheme which deviates substantially from the usual situation for antimony, suggesting a flipping between opposing bond orientations. All the mixed sites are distributed regularly along the sheared pseudohexagonal boundaries of the lozenge-shaped rods; none of them are in the rod interior. The bonding schemes of dominant Sb sites show remarkable similarity to those in monoclinic boulangerite (Mumme, 1989; Ventruti et al., 2012), in which the Sb sites show typical Sb coordination and elongated short-bond versions and in which these sites, including the peculiar Sb6 site (it has the same name in Ventruti et al., 2012), occur at the same structural sites and with about the same bond lengths. The analogue of the Sb5 site in the structure description by Mumme (1989) has bond lengths of 2.73, 2.82, 2.87, and 2.88 Å; in the description by Ventruti et al. (2012) the corresponding values are 2.74, 2.84, 2.80, and 2.90 Å; both coordinations in the pyramidal base are slightly larger than those in lopatkaite, in agreement with the larger structure volume of boulangerite. The bond distances to the pyramidal S vertex are typical for Sb – 2.48 and 2.43 Å, respectively – in these two refinements.

The Sb1 site, with somewhat elongated short basal distances (above), is in a rather symmetrically positioned central site of the double layer. It is surrounded by Pb coordination polyhedra and compensates for these distances by means of shortened long Sb–S distances (Table 6). Similar compensation occurs for the marginal Sb6 site.

Arsenic is preferentially concentrated at peripheral ribbon positions, where steric constraints favour incorporation of the smaller As^{3+} cation relative to Sb^{3+}. This distribution pattern is consistent with that observed in other Pb–Sb–As sulfosalts and reflects crystal–chemical control rather than random substitution (e.g. Moëlo et al., 2011; Biagioni and Moëlo, 2017).

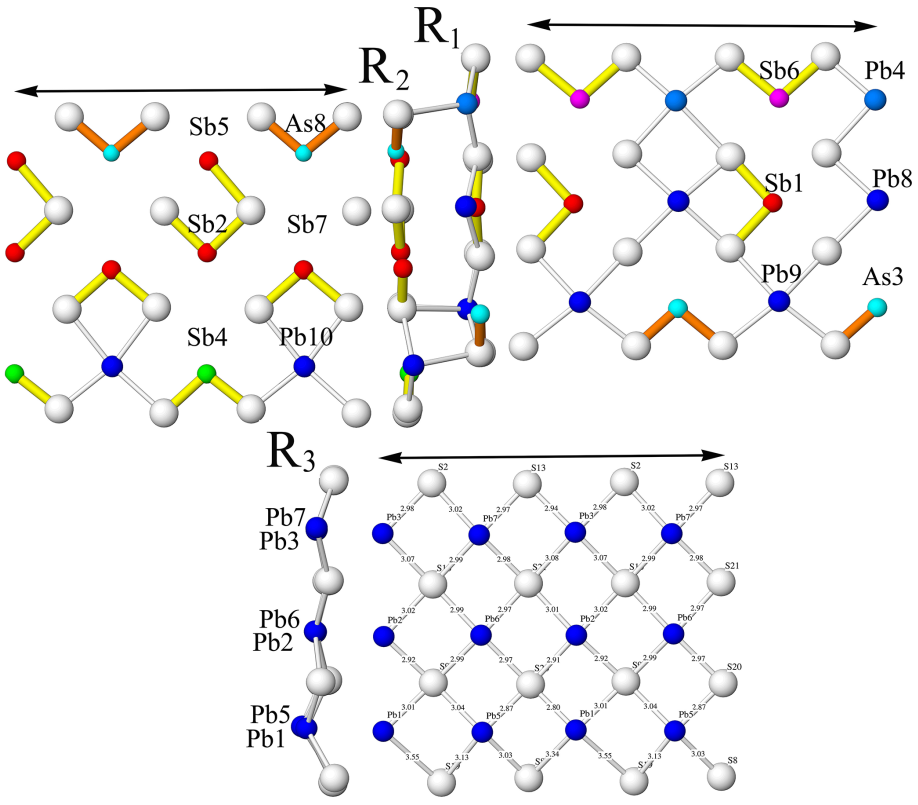

Figure 5. The R_1, R_2, and R_3 ribbons of the lopatkaite crystal structure oriented along the *a* axis (two unit cells, i.e. ~ 16 Å) showing the lack of crankshaft chains. Atom colouring is as in Fig. 2.

6 Discussion

The chemistry and the results of the crystal structure determination allow the calculation of a theoretical value of the arsenic content, which will define the border between As-bearing boulangerite and lopatkaite. Considering, theoretically, only two (As,Sb) sites with minimum $As_{0.505}Sb_{0.495}$ occupancy, the resulting formula is $Pb_{10}As_{1.1}Sb_{6.9}S_{22}$, and 2.23 wt % As is required. For two (As,Sb) sites with $As_{0.505}Sb_{0.495}$ occupancy and a third (Sb,As) site with $Sb_{0.6}As_{0.4}$ occupancy, the resulting formula is $Pb_{10}As_{1.5}Sb_{6.5}S_{22}$, which requires 3.05 wt % As. This suggests that a minimum of ~ 3 wt % As content is necessary for the formation of lopatkaite.

Based on more than 250 spot analyses of lopatkaite from the Madoc deposit, we found a range of chemistries, from low-As lopatkaite to high-As lopatkaite, with empirical formulae varying from $Pb_{10.48}As_{1.57}Sb_{6.10}S_{21.84}$ to $Pb_{10.39}As_{2.60}Sb_{5.03}S_{21.98}$. The values of (Sb + As), Pb / (Sb + As), and As/Sb for low- and high-As varieties range from 7.67, 1.37, and 0.26 to 7.62, 1.36, and 0.52, respectively. Two clear trends are observed: (1) Sb + As is less than the ideal value of 8, and (2) the Pb / (Sb + As) ratio is higher than the ideal value of 1.25 for ideal boulangerite, $Pb_{10}Sb_8S_{22}$. The deviation from ideal values of (Sb+As) and Pb / (Sb + As) also appears for chemistries of boulangerite and As-bearing boulangerite measured on Madoc material. The binary plots of As vs. Sb, Pb vs. (Sb + As), and Pb / (Sb + As) vs. Sb / (Sb + As) are shown in Fig. 6. A detailed explanation and discussion of these observations will be given in a future publication, which will include the results of lopatkaite studies of samples from other localities.

The comparison of empirical and structural formulae and unit-cell parameters for boulangerite and lopatkaite is presented in Table 7. The comparison of independent atom sites and site occupancies for the boulangerite group members is given in Table 8. In Mumme's refinement the site A5, assigned as the pure Pb site, shows Me–S distances consistent with a (Pb,Sb) site ,and the site A5′, assigned as the pure Sb site, shows Me–S distances consistent with a (Sb,Pb) site, in accordance with the results for A5 and A5′ sites of Ventruti's solution and in accordance with Pb4 and Sb6 sites of our refinement.

Lopatkaite and monoclinic boulangerite share the same space group ($P2_1/c$), topology, coordination environments, and rod-based structural architecture. No subgroup–supergroup relationship, symmetry reduction, or topological modification is observed. According to the definitions of Lima-de-Faria et al. (1990), the two minerals are therefore isotypic. The substitution of As for Sb does not alter the

Table 7. Comparative data for natural monoclinic boulangerite group* minerals obtained from EPMA and SCXRD data, with space group $P2_1/c$ and for $Z = 4$.

Mineral Location	Boulangerite[a] Boliden	Boulangerite[b] Bottino	Lopatkaite Madoc
Empirical formula	$Pb_{10.1}(Sb_{7.5}Bi_{0.56})(S,Se)_{22}$	$Pb_{9.78}(Sb_{8.18}As_{0.08})(S,Se)_{22}$	$Pb_{10.28}As_{1.74}Sb_{6.06}S_{21.92}$
ch[c], As / (Sb + Bi)	0.20, 0	0.34, 0.010	0.12, 0.287
Pb / (Sb + As + Bi)	1.253	1.184	1.318
Structural formula	$Pb_{10}Sb_8S_{22}$	$Pb_{10.15}Sb_{7.85}S_{22}$,	$Pb_{10.336}As_{1.567}Sb_{6.088}S_{22}$
ch[c], As / (Sb + Bi)	0, 0	−0.15, 0.0	−0.35 0.257
Pb / (Sb + As + Bi)	1.250	1.293	1.350
Cell parameters (Å)			
a	8.084(3)	8.079(2)	8.0806(6)
b	23.543(8)	23.454(4)	23.3597(18)
c	21.612(7)	21.554(4)	21.4880(6)
β (°)	100.71(2)	100.76(1)	100.7090(10)
V (Å^3)	4041.58	4012(1)	3985.4(5)
R_1 factor (%)	13	6.2	4.12
Ref[d]	1	2	3

A monoclinic natural boulangerite group has not been officially defined yet, but a structural one (containing both synthetic and natural phases) was proposed by Ventruti et al. (2012). [a] In our notation; Mumme's original notation: $P2_1/a$, with $a = 21.612$, $b = 23.543$, $c = 8.084$ Å, and $\beta = 100.71°$. [b] In our notation; Ventruti's original notation: $P2_1/a$, with $a = 21.554$, $b = 23.454$, $c = 8.079$ Å, and $\beta = 100.76°$. [c] *ch* denotes charge-balanced values calculated as (Σ*cation valence* − Σ*anion valence*) using apfu values. [d] 1: Mumme (1989); 2: Ventruti et al. (2012); 3: this study

Table 8. Comparison of independent atom sites and site occupancies for the boulangerite group members (M: Mumme, 1989; V: Ventruti et al., 2012).

Boulangerite	Boulangerite M	Boulangerite V	Lopatkaite	Lopatkaite
Site	oc	oc	oc	Site
A1	$Pb_{1.00}$	$Pb_{1.00}$	$Pb_{1.00}$	Pb1
A2	$Pb_{1.00}$	$Pb_{1.00}$	$Pb_{1.00}$	Pb2
A3	$Pb_{1.00}$	$Pb_{1.00}$	$Pb_{1.00}$	Pb3
A5	$Pb_{1.00}$	$Pb_{0.69(10)}Sb_{0.31}$	$Pb_{0.926(8)}Sb_{0.074}$	Pb4
A1′	$Pb_{1.00}$	$Pb_{1.00}$	$Pb_{1.00}$	Pb5
A2′	$Pb_{1.00}$	$Pb_{1.00}$	$Pb_{1.00}$	Pb6
A3′	$Pb_{1.00}$	$Pb_{1.00}$	$Pb_{1.00}$	Pb7
A4′	$Pb_{1.00}$	$Pb_{1.00}$	$Pb_{1.00}$	Pb8
A7′	$Pb_{1.00}$	$Pb_{1.00}$	$Pb_{1.00}$	Pb9
A8′	$Pb_{1.00}$	$Pb_{1.00}$	$Pb_{1.00}$	Pb10
A4	$Sb_{1.00}$	$Sb_{1.00}$	$Sb_{1.00}$	Sb1
A6	$Sb_{1.00}$	$Sb_{1.00}$	$Sb_{1.00}$	Sb2
A7	$Sb_{1.00}$	$Sb_{1.00}$	$\mathbf{As_{0.671}}(16)Sb_{0.329}$	As3
A8	$Sb_{1.00}$	$Sb_{1.00}$	$Sb_{0.719(15)}As_{0.281}$	Sb4
A9	$Sb_{1.00}$	$Sb_{1.00}$	$Sb_{0.889(9)}Pb_{0.111}$	Sb5
A5′	$Sb_{1.00}$	$Sb_{0.54(13)}Pb_{0.46}$	$Sb_{0.690(9)}Pb_{0.310}$	Sb6
A6′	$Sb_{1.00}$	$Sb_{1.00}$	$Sb_{0.959(15)}As_{0.041}$	Sb7
A9′	$Sb_{1.00}$	$Sb_{1.00}$	$\mathbf{As_{0.576}}(16)Sb_{0.424}$	As8
Structural formula	$Pb_{10}Sb_8S_{22}$	$Pb_{10.15}Sb_{7.85}S_{22}$	$Pb_{10.336}As_{1.567}Sb_{6.088}S_{22}$	
Pb / (Sb + As)	1.250	1.293	1.350	

structural type. In the studied material, arsenic is dominant over antimony at two crystallographically independent mixed (Sb,As) sites. Under the dominant-constituent rule adopted by the IMA–CNMNC, such site dominance is sufficient to define a new mineral species, even when the overall structure remains unchanged. The ideal end-member composition of lopatkaite is thus $Pb_{10}As_2Sb_6S_{22}$, representing the arsenic-dominant isotype of boulangerite. Intermediate compositions reflect continuous As–Sb substitution within the same structural framework; however, species definition is based on site

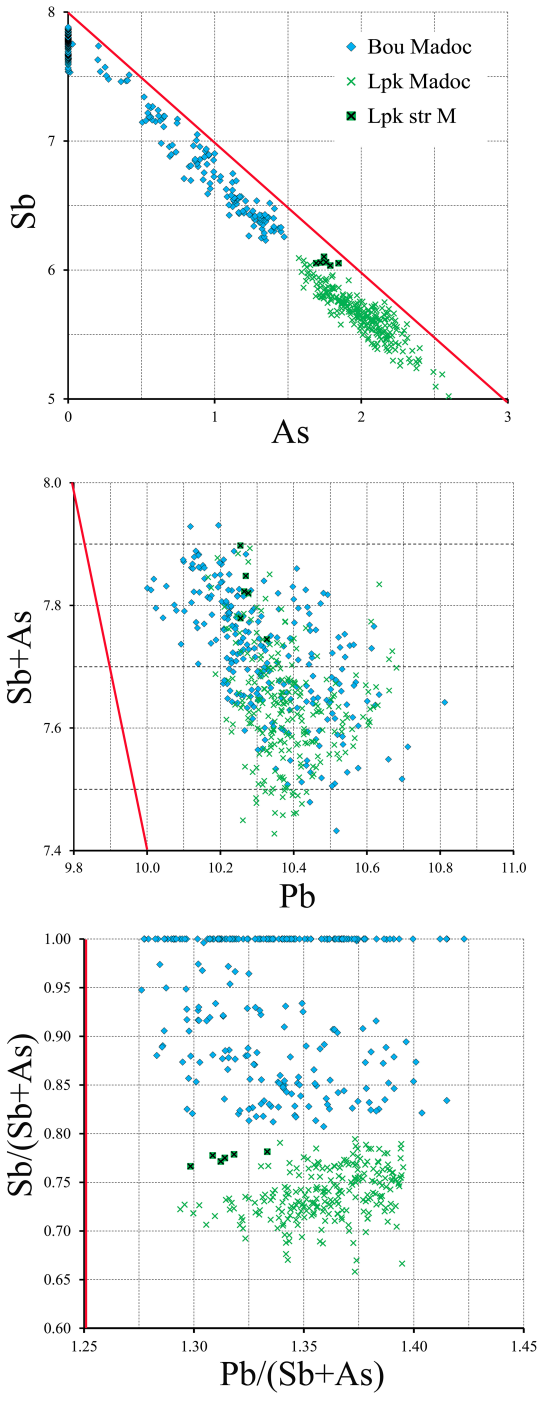

Figure 6. Binary plots of As vs. Sb **(a)**, Pb vs. (Sb + As) **(b)**, and Pb / (Sb + As) vs. Sb / (Sb + As) **(c)** based on apfu values ($Z = 4$) for boulangerite, As-bearing boulangerite, and lopatkaite from the Madoc deposit. More than 500 spot analysis points demonstrate the deviation of these parameters from those calculated from the ideal boulangerite formula, indicated by red lines.

occupancy dominance. Textural observations (Fig. 1) show that lopatkaite is overgrown and partially replaced by boulangerite, indicating changes in As/Sb ratios during mineralisation. These features are consistent with the two-stage sulfosalt deposition model proposed for the Madoc deposit (Jambor et al., 1982).

Lopatkaite is a pure Pb–Sb–As rod-based-structure sulfosalt mineral. It is an isotype of boulangerite with two structurally distinct cation sites, predominantly arsenic-occupied, and one more in a reversed ratio with Sb (Table 8). The above-described distribution of As in the rod volume, always under rod surfaces running diagonally to the crystal axes (Fig. 3), influences both the b and c parameters and, more strongly, the b parameter (Table 7). The unit-cell parameters are correspondingly reduced in relation to boulangerite (Table 7). The monoclinic boulangerite studied by Mumme (1989) has a 21.61 Å, b 23.54 Å, c 8.08 Å, β 100.71°, and space group $P2_1/a$ compared with our values of a 8.0806 Å, b 23.360 Å, c 21.488 Å, β 100.709°, and space group $P2_1/c$. With respect to the discussion about the symmetry and space group of synthetic and natural boulangerite in the literature (*Pbnm*, Petrova et al., 1978; *Pnam*, Skowron and Brown, 1990; $P2_1/c$; Mumme, 1989; Ventruti et al., 2012), lopatkaite is unambiguously on the side of the ordered structures and monoclinic symmetry.

After the approval of the lopatkaite proposal (January 2013), we determined further occurrences of lopatkaite (based on EPMA data and crystal structure determinations) at two other localities: the Barika gold deposit, Azerbaijan Province, Iran, and the Balmat deposit, New York, USA. Kasatkin et al. (2022) described lopatkaite with 3.08 wt % As from the Vorontsovskoe deposit, Russia, and Biagioni et al. (2025) reported lopatkaite with 3.8 wt % As from the Jas Roux deposit, France, with both identifications being based on EPMA data. Although Birnie and Petersen (1977), who studied As-rich "boulangerite" samples from Huachocolpa, Peru, indicated an As / (As + Sb) ratio of only 0.36, without giving explicit EPMA data, one can assume based on the calculated 5.97 As wt % content of their samples that they represent the first analytical data of lopatkaite. A comparative study of our newly determined lopatkaite occurrences and these literature data will be the subject of a separate paper.

Data availability. Crystallographic data for lopatkaite are available in the Supplement in Files S1 and S2.

Supplement. The supplement related to this article is available online at https://doi.org/10.5194/ejm-38-217-2026-supplement.

Author contributions. DT initiated the project. DT performed the EPMA and SCXRD experiments. EM interpreted the single-crystal data, and HP and GZ performed the optical measurements.

The paper was written by DT with contributions from all of the co-authors.

Competing interests. The contact author has declared that none of the authors has any competing interests.

Disclaimer. Publisher's note: Copernicus Publications remains neutral with regard to jurisdictional claims made in the text, published maps, institutional affiliations, or any other geographical representation in this paper. The authors bear the ultimate responsibility for providing appropriate place names. Views expressed in the text are those of the authors and do not necessarily reflect the views of the publisher.

Acknowledgements. The authors express their gratitude to Eduard Lopatka for the material donated, to Goran Batic for the help with the sample preparation, and to Uwe Kolitsch for the helpful comments. We thank the editor, Luca Bindi, for handling the paper, and thanks are given to Yves Moëlo and to one anonymous reviewer for their critical remarks that have improve the paper.

Review statement. This paper was edited by Luca Bindi and reviewed by Yves Moëlo and one anonymous referee.

References

Biagioni, C. and Moëlo, Y.: Lead-antimony sulfosalts from Tuscany (Italy). XIX. Crystal chemistry of chovanite from two new occurences in the Apuan Alps and its 8 Å crystal structure, Min. Mag., 81, 811–831, https://doi.org/10.1180/minmag.2016.080.134, 2017.

Biagioni, C., Moëlo, Y., Orlandi, P., and Stanley, C.: Lead-antimony sulfosalts from Tuscany (Italy). XVII.: Meerschautite, $(Ag,Cu)_{5.5}Pb_{42.4}(Sb,As)_{45.1}S_{112}O_{0.8}$, a new expanded derivative of owyheeite from the Pollone mine, Valdicastello Carducci: Occurrence and crystal structure, Min. Mag., 80, 675–690, https://doi.org/10.1180/minmag.2016.080.011, 2016.

Biagioni, C., Moëlo, Y., Orlandi, P., and Paar, W.: Lead-antimony sulfosalts from Tuscany (Italy). XXIII. Andreadinite, $CuAg_7HgPb_7Sb_{24}S_{48}$, a new oversubstituted (Cu,Hg)-rich member of the andorite homeotypic series from Monte Arsiccio mine, Apuan Alps, Eur. J. Mineral., 30, 1021–1035, https://doi.org/10.1127/ejm/2018/0030-2765, 2018.

Biagioni, C., Bindi, L., Momma, K., Miyawaki, R., Matsushita, Y., and Moëlo, Y.: Determination of the crystal structure and redefinition of tsugaruite, $Pb_{28}As_{15}S_{50}Cl$, the first lead-arsenic chloro-sulfosalt, Can. Miner., 59, 125–137, https://doi.org/10.3749/canmin.2000005, 2021.

Biagioni, C., Sejkora, J., Moëlo, Y., Favreau, G., Bourgoin, V., Boulliard, J.-C., Bonaccorsi, E., Mauro, D., Musetti, S., Pasero, M., Perchiazzi, N., and Ulmanová, J.: Ginelfite, $Ag_2(Ag_{0.5}Fe_{0.5})TlPb_{24.5}(Sb,As)_{32.5}S_{75.5}$, a new boxwork sulfosalt from Jas Roux, France: occurrence and crystal structure, Eur. J. Mineral., 37, 319–335, https://doi.org/10.5194/ejm-37-319-2025, 2025.

Bindi, L., Biagioni, C., Martini, B., and Salvetti, A.: Ciriottiite,$Cu(Cu,Ag)_3Pb_{19}(Sb,As)_{22}(As_2)S_{56}$, the Cu-analogue of sterryite from the Tavagnasco Mining District, Piedmont, Italy, Minerals, 6, 8, https://doi.org/10.3390/min6010008, 2016.

Birnie, R. W. and Petersen, U.: The paragenetic Association and Compositional Zoning of Lead Sulfosalts at Huachocolpa, Peru, Econ. Geol., 72, 983–992, 1977.

Bruker AXS: SHELXTL, Version 5.1, Bruker AXS, Inc., Madison,WI 53719, USA, 1997.

Bruker AXS: SMART, Version 5.0, Bruker AXS, Inc., Madison, WI 53719, USA, 1998a.

Bruker AXS: SAINT, Version 5.0, Bruker AXS, Inc., Madison, WI 53719, USA, 1998b.

Ferraris, G., Makovicky, E., and Merlino, S.: Crystallography of Modular Materials, IUCr Monographs on Crystallography 15, Oxford University Press, Oxford, U.K., ISBN 978-0-19-954569-8, 2008.

Garavelli, A., Mozgova, N., Orlandi, P., Bonaccorsi, E., Pinto, D., Moëlo, Y., and Borodaev, Y.: Rare sulfosalts from Vulcano, Aeolian Islands, Italy. V. Vurroite, $Pb_{20}Sn_2(Bi,As)_{22}S_{54}Cl_6$, a new mineral species, Can. Mineral., 45, 703–711, https://doi.org/10.2113/gscanmin.43.2.703, 2005.

Harris, D. C.: The mineralogy and geochemistry of the Hemlo gold deposit, Ontario, Geological Survey of Canada, Economic Geology, Report 38, 1989.

Ilinca, G.: Charge Distribution and Bond Valence Sum Analysis of Sulfosalts – The ECoN21 Computer Program, Minerals, 12, 924, https://doi.org/10.3390/min12080924, 2022.

Jambor, J. L.: New lead sulfantimonides from Madoc, Ontario. Part I, Can. Mineral., 9, 7–24, 1967a.

Jambor, J. L.: New lead sulfantimonides from Madoc, Ontario. Part II, Can. Mineral., 9, 191–213, 1967b.

Jambor, J. L., Laflamme, J. H. G., and Walker, D. A.: A re-examination of the Madoc sulfosalts, Mineral. Rec., 13, 93–100, 1982.

Johan, Z. and Mantienne, J.: Thallium-rich mineralization at Jas Roux, Hautes-Alpes, France: a complex epithermal, sediment-hosted, ore-forming system, Journal of the Czech Geological Society, 45/1–2, 63–77, 2000.

Kasatkin, A. V., Stepanov, S. Yu, Tsyganko, M. V., Škoda, R., Nestola, F., Plášil, J., Makovicky, E., Agakhanov, A. A., and Palamarchuk, R. S.: Mineralogy of the Vorontsovskoe gold deposit (Northern Urals), Mineralogiya [Mineralogy], 8, 5–93, https://doi.org/10.35597/2313-545X-2022-8-1-1, 2022.

Kraus, W. and Nolze, G.: POWDER CELL-A Program for the Representation and Manipulation of Crystal Structure and Calculation of the Resulting X-Ray Powder Pattern, J. Appl. Crystallogr., 29, 301–303, https://doi.org/10.1107/S0021889895014920, 1996.

Lima-de-Faria, J., Heller, E., Liebau, F., Makovicky, E., and Parthe, E.: Report of the International Union of Crystallography Commission on Crystallographic. Nomenclature Subcommittee on the Nomenclature of Inorganic Structure Types, Acta Cryst. A46, 1–11, https://doi.org/10.1107/S0108767389008834, 1990.

Makovicky, E.: Rod-based sulphosalt structures derived from the SnS and PbS archetypes, Eur. J. Mineral., 5, 545–591, https://doi.org/10.1127/ejm/5/3/0545, 1993.

Moëlo, Y., Makovicky, E., Mozgova, N. N., Jambor, J. L., Cook, N., Pring, A., Paar, W. H., Nickel, E. H., Graeser, S., Karup-Møller, S., Balić-Žunić, T., Mumme, W. G., Vurro, F., Topa, D., Bindi, L., Bente, K., and Shimizu, M.: Sulfosalt systematics: a review. Report of the sulfosalt sub-committee of the IMA Commission on Ore Mineralogy, Eur. J. Mineral., 20, 7–46, https://doi.org/10.1127/0935-1221/2008/0020-1778, 2008.

Moëlo, Y., Orlandi, P., Guillot-Deudon, C., Biagioni, C., Paar, W., and Evain, M.: Lead-antimony sulfosalts from Tuscany (Italy). XI. The new mineral species parasterryite, $Ag_4Pb_{20}(Sb_{14.5}As_{9.5})S_{24}S_{58}$, and associated sterryite, $Cu(Ag,Cu)_3Pb_{19}(Sb,As)_{22}(As–As)S_{56}$, from the Pollone mine, Tuscany, Italy. Can. Mineral., 49, 623–638, https://doi.org/10.3749/canmin.49.2.623, 2011.

Mumme, W. G.: The crystal structure of $Pb_{5.05}(Sb_{3.75}Bi_{0.28})S_{10.72}Se_{0.28}$: boulangerite of near ideal composition, Neues Jahrbuch für Mineralogie, Monatshefte, 11, 498–512, 1989.

Orlandi, P., Moëlo, Y., and Biagioni, C.: Jamesonite delle miniere di Fornovolasco (Vergemoli, Lucca): primo ritrovamento sulle Alpi Apuane, Atti Soc. tosc. Sci. nat., Mem., 113, 89–95, 2008.

Petrova, I. V., Kuznetsov, A. I., Belokoneva, Ye. E., Simonov, M. A., Pobedimskaya, Ye. A., and Belov, N. V.: On the crystal structure of boulangerite, Doklady Akademii Nauk SSSR, 242, 337–340, 1978.

Shimizu, M., Miyawaki, R., Kato, A., Matsubara, S., Matsuyama, F., and Kiyota, K.: Tsugaruite, $Pb_4As_2S_7$, a new mineral species from the Yunosawa mine, Aomori Prefecture, Japan, Min. Mag., 62, 793–799, https://doi.org/10.1180/002646198548179, 1998.

Skowron, A. and Brown, I. D.: Refinement of the structure of boulangerite, $Pb_5Sb_4S_{11}$, Acta Cryst., C46, 531–534, https://doi.org/10.1107/S0108270189008334, 1990.

Topa, D., Makovicky, E., Putz, H., and Zagler, G.: Lopatkaite, IMA 2012-083. CNMNC Newsletter No. 15, Min. Mag., 77, 11, https://doi.org/10.1180/minmag.2013.077.1.01, 2013.

Topa, D., Stoeger, B., Keutsch, F. N., and Ilinca, G.: The crystal structure of launayite from Taylor Pit, Madoc, Ontario, Canada: crystal chemistry, modulated superstructures, and parent modular structure compared with rouxelite, Eur. J. Mineral., 37, 971–994, https://doi.org/10.5194/ejm-37-971-2025, 2025.

Ventruti, G., Stasi, F., Pinto, D., Vurro, F., and Renna, M.: The plumose boulangerite from Bottino, Apuan Alps, Italy, Crystal structure, OD character and twinning, Can. Mineral., 50, 181–199, https://doi.org/10.3749/canmin.50.2.181, 2012.

Zelenski, M., Garavelli, A., Pinto D., Vurro, F., Moëlo, Y., Bindi, L., Makovicky, E., and Bonaccorsi, E.: Tazieffite, $Pb_{20}Cd_2(As,Bi)_{22}S_{50}Cl_{10}$, a new chloro-sulfosalt from Mutnovsky volcano, Kamchatka Peninsula, Russian Federation, Am. Mineral., 94, 1312–1324, https://doi.org/10.2138/am.2009.3190, 2009.